Generalized Allen-Cahn equations to describe far-from-equilibrium order-disorder dynamics

J.-F. Gouyet*
Laboratoire de Physique de la Matière Condensée, Ecole Polytechnique, F-91128 Palaiseau, France
(Received 21 December 1993; revised manuscript received 28 September 1994)

We examine in some detail the mean-field discrete lattice gases with repulsive interactions with the purpose of establishing generalized Allen-Cahn equations to describe far-from-equilibrium order-disorder dynamics in the same spirit as our previous study for the attractive case which led to a generalized Cahn-Hilliard equation. The starting point is the general master equation, and all analytic developments are done within the framework of mean-field theory, using the most natural averaging approximation. As applications we determine the analytic forms of the antiphase boundaries velocity for the square and the simple cubic lattices, and we show that the conductivity always increases along these antiphase boundaries.

PACS number(s): 05.50.+q, 64.60.Cn, 68.35.Fx, 64.60.My

I. INTRODUCTION

Lattice-gas models have found numerous applications in the thermodynamics of alloys and nonstoichiometric compounds [1]. Lattice gases with repulsive interactions are of particular interest in studies of transport properties of superionic conductors [2], intercalation processes in rigid host structures [3], or surface diffusion with formation of ordered states [4].

When we want to study the dynamics of diffusion with inhomogeneous concentration profiles in the presence of an order-disorder transition [5], it turns out that the usual phenomenological Allen-Cahn approach can no longer be applied, as it is based upon linear assumptions of the Onsager type. In this case, the effective diffusion coefficient depends not only on the average local concentration, but also on the concentration gradients, on the local order parameter, and on the distribution of antiphase boundaries (see Fig. 1). In addition a notion of a dynamical phase diagram must be introduced as the phase diagram itself depends, among other things, on the concentration gradient (finite gradient effect) [6]. If the general behavior is relatively well known, there exists to our knowledge no detailed mean-field study of the far-from-equilibrium order-disorder dynamics on discrete lattices, starting not from phenomenological assumptions, but directly from the master equation itself.

Therefore, this paper is specifically devoted to a general mean-field approach of the far-from-equilibrium dynamics of lattice gases in the hopping regime with nearest neighbor *repulsive* interaction, embedded in a thermal bath fixing its temperature, with a special emphasis on its relation with thermodynamics [7,8] and with area preserving maps [9]. Using an approach previously developed by Martin in the one-dimensional attractive case, and in any dimensions by Gouyet [10], we shall be able to establish a generalized set of coupled nonphenomenological Allen-Cahn equations [11], not restricted to the vicinity of the equilibrium state. As examples of applications of this approach, we shall calculate the analytic form of the velocity of antiphase boundaries (in the case of square and simple cubic lattices), and we shall show that the conductivity increases in the antiphase boundaries.

To establish this set of coupled equations we must first notice that in the case of nearest neighbor repulsive in-

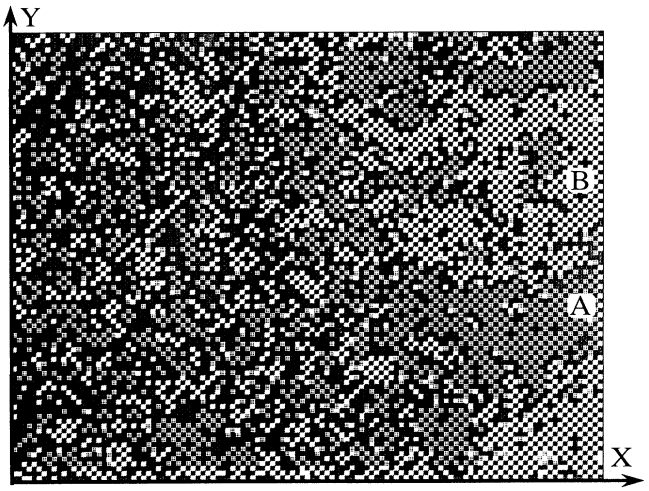

FIG. 1. Monte Carlo simulation of a diffusion process of repulsive particles on a square lattice at a temperature smaller than T_c. The diffusion gradient is along the direction x, the concentration decreasing with x. There exists a range of concentration where an ordering appears, developing two checkerboard substructures A and B ("colors"). In these ordered regions many defects (particles or vacancies) are present, in particular, at the border of the domains. We have colored the B sites in grey to show the domains: when black particles are on sites A (A domain), the picture looks black and grey when the black particles are on B sites (B domains), the picture looks black and white. Black regions are regions with particle defects, white and grey regions are regions with vacancy defects.

*Electronic address: jfg@pmcsun1.polytechnique.fr

teractions, most discrete lattices favor the appearance of an order-disorder transition in which the lattice symmetry is broken. The order discriminates different sublattices which can be indexed by a "color." For instance, in the case of the square lattice, the order discriminates two sublattices with colors A and B, which have a checkerboard structure. We shall concentrate here our attention on the square lattice (with $z=4$ nearest neighbors) and on the simple cubic lattice ($z=6$), but the approach can be easily generalized to any lattice structure (the case of a triangular lattice, with an application to intercalation in $TiSe_2$ is in progress [12]). In the present case, the study leads to sets of discrete coupled kinetic equations for the concentrations of particles of the two colors A and B. They are deduced from the master equation describing the kinetics, in the same spirit as the case of attractive interactions [10].

II. THE LATTICE-GAS MODEL

The general master equation for the kinetic evolution of the average concentration $p_{\mathbf{k}}=\langle n_k\rangle$ at site $\mathbf{k}$ can be written

$$\frac{\partial p_{\mathbf{k}}}{\partial t}\equiv\frac{\partial}{\partial t}\langle n_{\mathbf{k}}\rangle=\sum_{\mathbf{j}}\langle w_{\mathbf{jk}}(\{n\})n_{\mathbf{j}}(1-n_{\mathbf{k}})-w_{\mathbf{kj}}(\{n\})\times n_{\mathbf{k}}(1-n_{\mathbf{j}})\rangle\ , \tag{1}$$

where $n_{\mathbf{k}}=0,1$ is the occupation number of site $\mathbf{k}$ and $w_{\mathbf{ij}}(\{n\})$ is the jump probability operator from site $\mathbf{i}$ to site $\mathbf{j}$, which depends on the environment (given by the configuration $\{n\}$). The definition of $p_{\mathbf{k}}$ supposes a sample averaging in which the boundaries are (in average) pinned at the same position by the noise (we do not adopt the coarse graining averaging). For simplicity, the jumps are supposed to be limited to nearest neighbor sites $\mathbf{k}+\mathbf{a}'$ of any site $\mathbf{k}$. It is then convenient to introduce a current operator $\mathcal{J}_{\mathbf{k},\mathbf{k}+\mathbf{a}}(\{n\})$ along the link $\mathbf{k}\rightarrow\mathbf{k}+\mathbf{a}$, so that Eq. (1) becomes

$$\frac{\partial p_{\mathbf{k}}}{\partial t}=-\sum_{\mathbf{a}}\langle\mathcal{J}_{\mathbf{k},\mathbf{k}+\mathbf{a}}(\{n\})\rangle \tag{2}$$

[where we have taken $\mathbf{j}=\mathbf{k}+\mathbf{a}$ in Eq. (1)]. The average current in the bond $(\mathbf{i},\mathbf{j})$ is

$$J_{\mathbf{ij}}(\{p\})\equiv\langle\mathcal{J}_{\mathbf{ij}}(\{n\})\rangle=\langle w_{\mathbf{ij}}n_{\mathbf{i}}(1-n_{\mathbf{j}})-w_{\mathbf{ji}}n_{\mathbf{j}}(1-n_{\mathbf{i}})\rangle\ . \tag{3}$$

We are interested here in lattice gases with repulsive interactions for which an order-disorder transition appears at some critical temperature T_c. As indicated above, on the square and simple cubic lattice the symmetry breaking is between two sublattices $\{A\}$ and $\{B\}$ that will be distinguished by their colors A and B (Fig. 1). The occupation probabilities on these sublattices will be identified with an upper index A or B, $\mathbf{i}\in\{A\}$ and $\mathbf{j}\in\{B\}$; $\mathbf{k}$ will designate any site $\mathbf{i}$ or $\mathbf{j}$. Equations (2) and (3) then become

$$\frac{\partial p_{\mathbf{i}}^{A}}{\partial t}=-\sum_{\mathbf{j}=\mathbf{i}+\mathbf{a}}\langle\mathcal{J}_{\mathbf{ij}}^{AB}(\{n\})\rangle\ ,\qquad \frac{\partial p_{\mathbf{j}}^{B}}{\partial t}=-\sum_{\mathbf{i}=\mathbf{j}+\mathbf{a}}\langle\mathcal{J}_{\mathbf{ji}}^{BA}(\{n\})\rangle\ , \tag{4}$$

with a current defined by

$$J_{\mathbf{ij}}^{AB}\equiv\langle\mathcal{J}_{\mathbf{ij}}^{AB}(\{n\})\rangle=\langle w_{\mathbf{ij}}^{AB}n_{\mathbf{i}}^{A}(1-n_{\mathbf{j}}^{B})-w_{\mathbf{ji}}^{BA}n_{\mathbf{j}}^{B}(1-n_{\mathbf{i}}^{A})\rangle. \tag{5}$$

As the designation of the colors A and B is arbitrary, it is very convenient to consider simultaneously the two color cases for each site $\mathbf{k}$: this allows us to define on each site $\mathbf{k}$ both concentrations $p_{\mathbf{k}}^{A}$ and $p_{\mathbf{k}}^{B}$. It corresponds to averaging at each time two extremely close realizations of the ordering process. With these definitions (that is, satisfying the symmetry between the sublattices) for the master equation driving the two concentrations $p_{\mathbf{k}}^{A}$ and $p_{\mathbf{k}}^{B}$, the two concentrations will vary smoothly on the whole lattice [13]. This remark is based on the fact that in the absence of any chaotic regime two concentrations $p_{\mathbf{k}}^{A}$ and $p_{\mathbf{k}+\mathbf{a}}^{A}$ close at the initial time will remain close at all time. This point is detailed in Appendix A.

The choice of the averaging procedure for the mean-field treatment can follow various physical or practical (i.e., numerical) motivations. It will be chosen here to lead to the usual thermodynamic approach (case I of Ref. [10]). A convenient average takes the form

$$J_{\mathbf{ij}}^{AB}(\{p\})=\langle\tilde{w}_{\mathbf{ij}}^{AB}\rangle p_{\mathbf{i}}^{A}(1-p_{\mathbf{j}}^{B})-\langle\tilde{w}_{\mathbf{ji}}^{BA}\rangle p_{\mathbf{j}}^{B}(1-p_{\mathbf{i}}^{A})\ , \tag{6}$$

$\tilde{w}_{\mathbf{ij}}$ being derived from $w_{\mathbf{ij}}(\{n\})$ with some arbitrariness, taking into account the presence of the $n_{\mathbf{i}}(1-n_{\mathbf{j}})$ operator and the relation $n_{\mathbf{k}}=n_{\mathbf{k}}^{2}$. We will turn this arbitrariness to account, to choose $\tilde{w}_{\mathbf{ij}}$ in agreement with the well-established thermodynamics (see also Ref. [10]).

In most applications, the host potential in which the hopping particles diffuse can be seen as an egg-box potential. The associated lattice is the lattice of the potential minima. The bonds join nearest sites through a saddle point. The jump probabilities $w_{\mathbf{ij}}(\{n\})$ in a lattice gas hopping model (Eyring absolute regime) are then essentially a function of the energy difference, seen by the jumping particle, between its initial well (site $\mathbf{k}$) and the saddle point (between $\mathbf{k}$ and $\mathbf{k}+\mathbf{a}$). Here we consider only a nearest neighbor interaction and the saddle point is supposed at a fixed (zero) energy, hence not sensitive to the occupation of the neighboring sites. The Hamiltonian of the system of diffusing particles for a given configuration $\{n\}$ (in the hopping model, the particles spend most of their time in the wells) is

$$\mathcal{H}=-\sum_{\mathbf{i},\mathbf{j}}\varepsilon_{\mathbf{ij}}^{AB}n_{\mathbf{i}}^{A}n_{\mathbf{j}}^{B}-\sum_{\mathbf{i}}\varepsilon_{\mathbf{i}}^{A}n_{\mathbf{i}}^{A}-\sum_{\mathbf{j}}\varepsilon_{\mathbf{j}}^{B}n_{\mathbf{j}}^{B}\ . \tag{7}$$

For a short range repulsive interaction $\varepsilon_{\mathbf{ij}}=\varepsilon<0$ with $\{i,j\}$ nearest neighbors and zero otherwise; in the following we will choose $\varepsilon_{\mathbf{i}}^{A}=\varepsilon_{\mathbf{j}}^{B}=\mu_e$, which corresponds to a

uniform lattice where all the sites are equivalent. With these conditions, the standard jump operator at temperature T, which leads to Arrhenius jump probabilities and Boltzmann equilibrium distribution is

$$\omega_{ij}^{AB}(\{n\})=w_0 \exp\left[-\frac{\varepsilon}{kT}\sum_{a'\neq j-i} n_{i+a'}^{B}\right], \tag{8a}$$

($w_0^A=w_0^B=w_0$ on a uniform lattice, is a constant prefactor, and the final site is considered empty in the expression of ω).

But the jump probability operator can be written in a different way [10],

$$\tilde{\omega}_{ij}^{AB}(\{n\})=w_0 \exp\left[s\frac{\varepsilon}{kT}n_j^B\right]\exp\left[-\frac{\varepsilon}{kT}\sum_{a'} n_{i+a'}^{B}\right], \tag{8b}$$

which is equivalent to (8a), due to the presence in (1) of the operator $(1-n_j)$: it is identical to (8a) when $n_j=0$, and with zero contribution when $n_j=1$; $s=1$ gives ω^{AB} where the arrival site of the jumping particle is excluded from the sum. The interest of introducing the parameters will appear later. It is for the moment arbitrary.

Mean-field approach

In the mean-field approximation, all the operators n_k in the expressions for the jump probabilities $w_{k,k+a}$ are replaced by their average concentrations p_k. Depending on the explicit form of the jump operators, different approximations can be obtained.

The general expression for the current can then be written

$$J_{ij}^{AB}(\{p\})=w_0\left\{w_r(p_j^B)^{-s}\prod_{a'} w_r(p_{i+a'}^B)p_i^A(1-p_j^B)-w_r(p_i^A)^{-s}\prod_{a'} w_r(p_{j+a'}^A)p_j^B(1-p_i^A)\right\}, \tag{9}$$

where $w_r(p_i^A)=\langle \exp-(\varepsilon/kT)n_i^A\rangle$ is the contribution of the occupation of site i to the jump probability. A similar expression is obtained for $J_{ji}^{BA}(\{p\})$.

As already noticed above, we will take the average in the exponential for w_r; this average leads to the usual thermodynamic equilibrium

$$w_r(p_i^A)=\exp\left[-\frac{\varepsilon}{kT}p_i^A\right]. \tag{10}$$

To conveniently introduce the thermodynamic variables one can proceed as in Ref. [10], factorizing the currents into a contribution S, symmetrical with respect to the initial and final states, and a factor which is the difference between a local function C invariant by the transformations of the local point group of symmetry, taken at the final j and initial i states,

$$J_{ij}^{AB}(\{p\})=-S_{ij}^{AB}(C_j^B-C_i^A). \tag{11}$$

This equation, together with the equations of evolution of the local concentrations (4) and (5), constitute our generalized Allen-Cahn equations.

After identification one finds (up to an arbitrary constant factor c_0)

$$C_i^A=c_0 w_r(p_i^A)^s\frac{p_i^A}{1-p_i^A}\prod_{a'} w_r(p_{i+a'}^B), \tag{12a}$$

$$S_{ij}^{AB}=\frac{w_0}{c_0}\frac{(1-p_i^A)(1-p_j^B)}{w_r(p_i^A)^s w_r(p_j^B)^s}. \tag{12b}$$

From (12a) it is possible to introduce what can be identified to a local chemical potential on each site $\{i,A\}$ or $\{j,B\}$

$$\mu_i^A=kT\ln C_i^A,\quad \mu_j^B=kT\ln C_j^B, \tag{13}$$

defined via Eqs. (10) and (12a) (c_0 has been chosen here such that $\mu_{k0}\Longrightarrow-\mu_{k0}$ when $p_k\Longrightarrow 1-p_k$) by

$$\mu_k^A=\mu_{k0}^A\equiv -s\varepsilon(p_k^A-\tfrac{1}{2})-z\varepsilon(p_k^B-\tfrac{1}{2})-\varepsilon\sum_{a'}\mathcal{D}_{a'}p_k^B+kT\ln\frac{p_k^A}{1-p_k^A}, \tag{14a}$$

$$\mu_k^B=\mu_{k0}^B\equiv -s\varepsilon(p_k^B-\tfrac{1}{2})-z\varepsilon(p_k^A-\tfrac{1}{2})-\varepsilon\sum_{a'}\mathcal{D}_{a'}p_k^A+kT\ln\frac{p_k^B}{1-p_k^B}. \tag{14b}$$

$\mathcal{D}_a$ is a difference operator defined by

$$\mathcal{D}_a f(\mathbf{k})=f(\mathbf{k}+\mathbf{a})-f(\mathbf{k}).$$

(The sum on a' in (14) is then a discrete Laplacian operator [14].)

The parameter s allows one here to distinguish between the usual chemical potential ($s=0$) when a particle is taken out of its site without jumping to a neighboring site, and a chemical potential taking into account the empty final state of a jump ($s=1$). A self-energy contribution must then be added to the chemical potential [see Eqs. (14a) and (14b)]. It seems possible to connect the parameter s with the expression of $c_1(1,\langle n\rangle)$, which appears in the density functional approach of the problem [15]. The site approximation is clearly not sufficient to determine s, and a contribution of the pair approximation is certainly necessary. The choice $s=0$, is, however, a choice which agrees at least with usual thermodynamics.

The quantities C^A and C^B are equivalent to *absolute*

activities [16]. Expressions (14) derived directly from the master Eqs. (4) and (5), can also be obtained as an extremum of a free energy $\langle F\rangle$ with the constraint of a fixed number of particles

$$\delta\left\{\langle F\rangle-\mu_1\left[\sum_i p_i^A+\sum_j p_j^B\right]\right\}=0\ ,$$

giving at equilibrium

$$\mu_1=\frac{\partial\langle F\rangle}{\partial p_i^A}=\mu_{i0}^A-\mu_e-\frac{z+s}{2}\varepsilon=\frac{\partial\langle F\rangle}{\partial p_j^B}=\mu_{j0}^B-\mu_e-\frac{z+s}{2}\varepsilon$$

with a free energy

$$\langle F\rangle=F_0+\sum_i\left[-\frac{\varepsilon}{2}\sum_a p_i^A p_{i+a}^B-s\frac{\varepsilon}{2}p_i^{A2}-\mu_e p_i^A+kT[p_i^A\ln p_i^A+(1-p_i^A)\ln(1-p_i^A)]\right]$$
$$+\sum_j\left[-\frac{\varepsilon}{2}\sum_a p_j^B p_{j+a}^A-s\frac{\varepsilon}{2}p_j^{B2}-\mu_e p_j^B+kT[p_j^B\ln p_j^B+(1-p_j^B)\ln(1-p_j^B)]\right]\ . \tag{15}$$

Remark. The symmetry between particles and holes, leading to relations (14), can be made visible by taking advantage of the arbitrariness (choice of the zero of energies) of μ_e (or of c_0): $\mu_e=kT\ln c_0=-(z+s/2)\varepsilon$ so that at equilibrium,

$$\mu_1=\frac{\partial\langle F\rangle}{\partial p_i^A}\equiv\mu_{i0}^A=\frac{\partial\langle F\rangle}{\partial p_j^B}\equiv\mu_{j0}^B\ . \tag{15a}$$

We now choose a situation with concentrations p_k^A and p_k^B defined on each site $\mathbf{k}$, and *slowly varying in space.* Introducing $\Delta F=2\{\langle F\rangle-F_0\}$ as a sum over *all* lattice sites $\mathbf{k}$

$$\Delta F=-\varepsilon\sum_{k,a}p_k^A p_{k+a}^B+\sum_k\left[-s\frac{\varepsilon}{2}p_k^{A2}-\mu_e p_k^A+kT[p_k^A\ln p_k^A+(1-p_k^A)\ln(1-p_k^A)]\right]$$
$$+\sum_k\left[-s\frac{\varepsilon}{2}p_k^{B2}-\mu_e p_k^B+kT[p_k^B\ln p_k^B+(1-p_k^B)\ln(1-p_k^B)]\right]\ . \tag{15b}$$

The form allows for the introduction of local quantities like the potential ϕ_k [Eq. (19) below]. Because (two) infinitesimally close realizations are treated simultaneously, $\langle F\rangle$ in Eq. (15b) is now multiplied by the number of sublattices (here 2). More generally, the number of independent concentrations on each site is equal to the number of sublattices (here p_k^A and p_k^B).

From relation (13), the current [Eq. (11)] can be written in a generalized Cahn-Hilliard form

$$J_{ij}^{AB}(\{p\})=-M_{ij}^{AB}(\mu_j^B-\mu_i^A)\ , \tag{11'}$$

with a mobility M, given in first approximation [which corresponds to a linearization of Eq. (11'), and a mobility in the equilibrium state] by

$$M_{ij}^{AB}(\{p\})\cong\beta S_{ij}^{AB}\sqrt{C_i^A C_j^B}\ . \tag{11''}$$

Far from equilibrium, the corrections due to the nonhomogeneous chemical potential are implicitly included in the mobility {using Eqs. (11), (13), and (11'); see also Eq. (12c) of Ref. [10]}.

We call Eq. (11'), together with Eq. (4) which gives the evolution of the concentrations as a function of the local currents [the explicit forms are written in Eqs. (37) and (40)], *generalized Allen-Cahn equations* for the following reasons.

In the (phenomenological) Allen-Cahn equation (AC) the kinetic equation {Eq. (11), Ref. [11]} is

$$\frac{\partial\eta}{\partial t}=-\alpha\frac{\delta\Delta F}{\delta\eta}\ ,$$

where η is the order parameter and we could see [using Eq. (20) below, and the relation $\eta=(p^A-p^B)/2$] that it gives the kinetic equation

$$\frac{\partial\eta}{\partial t}=-\alpha\frac{\delta\phi}{\delta\eta}-2\varepsilon\alpha\sum_{a'}\mathcal{D}_{a'}\eta\ ,$$

which has the form of Eq. (12) of Ref. [11]. But in the present study, (i) we obtain coupled equations which link the order parameter η to the mean concentration p (see below); (ii) the equations are no longer phenomenological (though only a mean-field approximation of the master equation).

As a consequence, the mobility M (α in [11]) contains new terms, functions of the gradients, and curvatures of the local concentrations (see Eq. (12c) in Ref. [10] for the simpler example of the generalized Cahn-Hilliard equation). As the only freedom during the derivation starting from the master equation is the use of the mean field, we expect the present equations to be valid far from equilibrium, because the master equation and its mean-field ap-

proximation are valid far from equilibrium.

Indeed, we could have also derived continuous equations from our discrete expressions. The discrete equations, involving five sites along each coordinate, the continuous equations will contain fourth-order derivatives or more exactly two-coupled second-order differential equations. This leads to complicated expressions without any practical gains (we nevertheless used the continuous limit to calculate the growth velocities). In addition, for numerical solutions of continuous differential equations needing discretization, this offers the best choice.

Before going into the details of the kinetic equations, we need to recall the main results concerning the phase diagram.

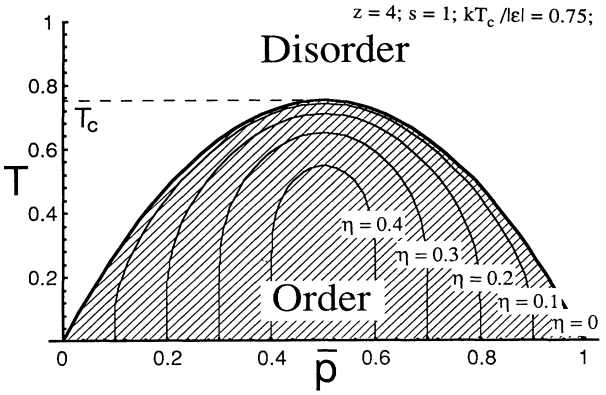

FIG. 2. Mean-field phase diagram. p is the local average concentration and η the local order parameter (here, $\varepsilon=-1$, $z=4$, $s=1$, $kT_c=0.75$).

III. THE ORDER-DISORDER TRANSITION

It is very easy to deduce the phase diagram of the order-disorder transition in the mean-field approximation from the above expressions. We need it here as a basis for the dynamics. This simple mean-field approximation leads to a qualitatively correct phase diagram. A better mean-field approach would consist in using the pair approximation such as the Kikuchi cluster variation method [17], or the real space renormalization group [18] (in calculating phase diagrams, the cluster variation method may in practice be more accurate than real space renormalization), while the best results can be obtained via Monte Carlo methods [9]. But it is not the purpose here to improve the results on statics: the use of the Sato and Kikuchi path probability method (derived from the cluster variation method) will be the subject of a work presently in progress.

The mean-field phase diagram can be obtained by setting the local currents to zero [Eq. (11)], in a homogeneous medium

$$p_{\mathbf{i}}^{A}\equiv p^{A} \text{ and } p_{\mathbf{j}}^{B}\equiv p^{B} \text{ for any } \mathbf{i} \text{ and } \mathbf{j} ,$$

and by laying down [using (11) and (13)] a fixed value to the chemical potentials, associated to a given temperature T and a fixed *average* concentration p_0

$$\mu_{\mathbf{i}}^{A}\equiv\mu_{\mathbf{j}}^{B}\equiv\mu_m \text{ for any } \mathbf{i} \text{ and } \mathbf{j} .$$

It is more suitable to change the variables and to introduce the local average concentration $p_{\mathbf{k}}$ and the local order parameter $\eta_{\mathbf{k}}$

$$p_{\mathbf{k}}\equiv\frac{p_{\mathbf{k}}^{A}+p_{\mathbf{k}}^{B}}{2} , \quad \eta_{\mathbf{k}}\equiv\frac{p_{\mathbf{k}}^{A}-p_{\mathbf{k}}^{B}}{2} . \tag{16}$$

The phase diagram is defined starting from Eq. (14) with $p_{\mathbf{k}}\equiv p=(p^{A}+p^{B})/2$ and $\eta_{\mathbf{k}}\equiv\eta=(p^{A}-p^{B})/2=0$, that is to say, by the equation

$$-s\varepsilon p^{A}-z\varepsilon p^{B}+kT\ln\frac{p^{A}}{1-p^{A}}=-s\varepsilon p^{B}-z\varepsilon p^{A}+kT\ln\frac{p^{B}}{1-p^{B}} . \tag{17a}$$

This equation is conveniently solved by considering the function

$$f(u)=(z-s)\varepsilon(u-\tfrac{1}{2})+kT\ln\frac{u}{1-u} , \tag{17b}$$

related to the chemical potentials of homogeneous concentrations by

$$\mu^{A}=f(p^{A})-2z\varepsilon(p-\tfrac{1}{2}) , \tag{17c}$$

$$\mu^{B}=f(p_B)-2z\varepsilon(p-\tfrac{1}{2}) , \tag{17d}$$

so that (17a) becomes

$$f(p^{A})=f(p^{B}) . \tag{17e}$$

A mean field phase diagram is shown in Fig. 2. This approximation is qualitatively comparable with the exact phase diagram. The diagram is symmetrical with respect to $p=\frac{1}{2}$; the critical mean-field temperature is $kT_c=-(z-s)\varepsilon/4$.

At equilibrium p is related to η by the equation [solving (17e)]

$$p=p_{\mathrm{eq}}(\eta,T)\equiv\tfrac{1}{2}\pm\left[(\tfrac{1}{2}-\eta)^2\left[\frac{2\eta}{\exp[-2\varepsilon(z-s)\eta/kT]-1}\right]\right]^{1/2} , \tag{18}$$

associated with a well-defined chemical potential, $\mu_m[p_{eq}(\eta,T),\eta]$ ($\mu_m[p_{eq}]$ is shown in Fig. 4).

IV. DOMAIN BOUNDARIES OF METASTABLE STATES

There exist metastable states associated with fixed uniform values of the chemical potential, in which the two-ordered phases are coexisting and separated by domain boundaries. These metastable states must have planar interfaces [11].

We first rewrite the free energy in its usual form of a (discrete) sum of a "ϕ^4" potential (we consider here its "exact" expression with the logarithms of the concentrations), and a quadratic term in the (discrete) gradient. Equation (15b) becomes

$$\Delta F=\sum_{\mathbf{k}}\left[\phi_{\mathbf{k}}+\frac{\varepsilon}{2}\sum_{\mathbf{a}}(\mathcal{D}_{\mathbf{a}}p_{\mathbf{k}}^{A})(\mathcal{D}_{\mathbf{a}}p_{\mathbf{k}}^{B})\right]$$

with

$$\phi_{\mathbf{k}}=\phi(p_{\mathbf{k}}^{A},p_{\mathbf{k}}^{B})=\phi_0-z\varepsilon p_{\mathbf{k}}^{A}p_{\mathbf{k}}^{B}-\mu_e p_{\mathbf{k}}^{A}-s\frac{\varepsilon}{2}p_{\mathbf{k}}^{A2}+kT[p_{\mathbf{k}}^{A}\ln p_{\mathbf{k}}^{A}+(1-p_{\mathbf{k}}^{A})\ln(1-p_{\mathbf{k}}^{A})]$$
$$-\mu_e p_{\mathbf{k}}^{B}-s\frac{\varepsilon}{2}p_{\mathbf{k}}^{B2}+kT[p_{\mathbf{k}}^{B}\ln p_{\mathbf{k}}^{B}+(1-p_{\mathbf{k}}^{B})\ln(1-p_{\mathbf{k}}^{B})]\ . \tag{19}$$

In the absence of an order-disorder transition the sublattices A and B are not differentiated ($\eta=0$, and $p_{\mathbf{k}}^{A}\equiv p_{\mathbf{k}}^{B}$) and (19) reduces to Eq. (16) of Ref. [10], except a common factor of two (the number of sublattices). Very generally the chemical potentials can be written from Eqs. (14), (15), and (19)

$$\mu_{\mathbf{k}}^{A}\equiv\frac{\partial\Delta F}{\partial p_{\mathbf{k}}^{A}}=\frac{\partial\phi_{\mathbf{k}}}{\partial p_{\mathbf{k}}^{A}}-\varepsilon\sum_{\mathbf{a}'}\mathcal{D}_{\mathbf{a}'}p_{\mathbf{k}}^{B}\ ,$$
$$\mu_{\mathbf{k}}^{B}\equiv\frac{\partial\Delta F}{\partial p_{\mathbf{k}}^{B}}=\frac{\partial\phi_{\mathbf{k}}}{\partial p_{\mathbf{k}}^{B}}-\varepsilon\sum_{\mathbf{a}'}\mathcal{D}_{\mathbf{a}'}p_{\mathbf{k}}^{A}\ . \tag{20}$$

The metastable and stable static states are then defined by the equations

$$\mu_{\mathbf{k}}^{A}\equiv\mu(p_{\mathbf{k}},\eta_{\mathbf{k}})=\mu_{\mathbf{k}}^{B}\equiv\mu(p_{\mathbf{k}},-\eta_{\mathbf{k}})=\mu\quad\text{for all }\mathbf{k}\ . \tag{21}$$

The chemical potential μ can be associated to a uniform concentration p_m^0 (larger than the average concentration p_0) for which the order parameter η is taken equal to zero. Using (14a) and (14b) together with $p_{\mathbf{k}}^{A}=p_{\mathbf{k}}^{B}\equiv p_m^0$), it is such that

$$\mu=-(z+s)\varepsilon(p_m^0-\tfrac{1}{2})+kT\ln\frac{p_m^0}{1-p_m^0}$$
$$\equiv f(p_m^0)-2z\varepsilon(p_m^0-\tfrac{1}{2})\ . \tag{22}$$

This concentration $p_m^0-p_0$ gives the amount of defects present in the antiphase boundaries with a good accuracy. We shall detail this point below.

On the other hand, quenching the system initially in equilibrium at high temperature with a homogeneous concentration $p_0(T_{\text{init}}\gg T_c)$ to a temperature $T(T<T_c)$ leads to an out-of-equilibrium situation where the chemical potential is at the beginning μ_0 given by

$$\mu_0=-(z+s)\varepsilon(p_0-\tfrac{1}{2})+kT\ln\frac{p_0}{1-p_0}\ . \tag{23}$$

This will be taken below as the initial state of the dynamical evolution. Figure 3 shows a construction using Eqs. (17b), (17c), and (17d) which gives, for a set (ε,T,p_0), the order parameter η, the chemical potential μ, and the concentration p_m^0. Figure 4 shows μ and μ_0 as a function of the average concentration p_0.

To study the evolution from this initial state, it is more convenient to work with the variables $\{p,\eta\}$ defined by (16):

$$\phi_{\mathbf{k}}=2\varepsilon\Phi(p_{\mathbf{k}},\eta_{\mathbf{k}})=\phi_0-2\mu_e p_{\mathbf{k}}-(z+s)\varepsilon p_{\mathbf{k}}^2+(z-s)\varepsilon\eta_{\mathbf{k}}^2$$
$$+kT\{(p_{\mathbf{k}}+\eta_{\mathbf{k}})\ln(p_{\mathbf{k}}+\eta_{\mathbf{k}})+(p_{\mathbf{k}}-\eta_{\mathbf{k}})\ln(p_{\mathbf{k}}-\eta_{\mathbf{k}})$$
$$+(1-p_{\mathbf{k}}-\eta_{\mathbf{k}})\ln(1-p_{\mathbf{k}}-\eta_{\mathbf{k}})+(1-p_{\mathbf{k}}+\eta_{\mathbf{k}})\ln(1-p_{\mathbf{k}}+\eta_{\mathbf{k}})\}\ . \tag{19'}$$

The surface Φ is symmetrical with respect to the plane $\eta=0$. The choice (15a) for μ_e gives Φ also symmetrical with respect to $p=\frac{1}{2}$ (particle-hole symmetry), while $\phi_0=-(z+s)\varepsilon/4+2kT\ln 2$ fixes the potential such that $\Phi(\frac{1}{2},0)=0$.

From (14a), (14b), and (19') it is possible to deduce the area-preserving mapping defining the interfaces at equilibrium associated with a given chemical potential μ. In general,

$$\sum_{\mathbf{a}}\mathcal{D}_{\mathbf{a}}p_{\mathbf{k}}=\frac{\partial\Phi}{\partial p_{\mathbf{k}}}-\frac{\mu_{\mathbf{k}}^{A}+\mu_{\mathbf{k}}^{B}}{2\varepsilon}\ ,$$
$$\sum_{\mathbf{a}}\mathcal{D}_{\mathbf{a}}\eta_{\mathbf{k}}=-\frac{\partial\Phi}{\partial\eta_{\mathbf{k}}}-\frac{\mu_{\mathbf{k}}^{A}-\mu_{\mathbf{k}}^{B}}{2\varepsilon}\ . \tag{24}$$

The terms on the left-hand sides of (24) are discrete Laplacian functions [14]. It is convenient here to introduce a "grand potential" Ψ defined by

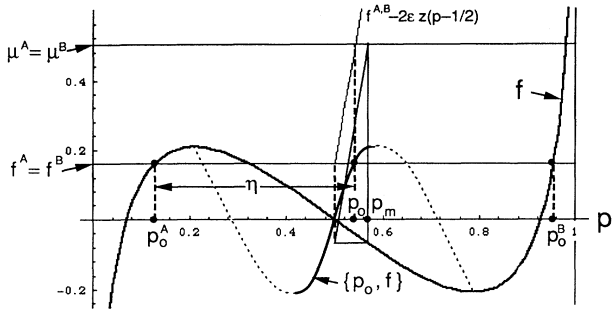

FIG. 3. Simple graphical construction at equilibrium of the order parameter η, of the chemical potential μ_m, and of the approximate interface concentration p_m^0, for a given mean concentration p_0 and a fixed temperature T: μ^A and μ^B, f^A and f^B, p_0^A and p_0^B are, respectively, the chemical potentials, the free energy, and the concentrations in the two ordered phases A and B corresponding to an average concentration p_0. The relation $f^{A,B}-2\varepsilon(p-\frac{1}{2})$ comes from Eq. (22) and gives μ.

$$\Psi(p_k,\eta_k,\mu,\delta\mu)=\Phi(p_k,\eta_k)-\frac{\mu}{\varepsilon}(p_k-\tfrac{1}{2})-\frac{\delta\mu}{\varepsilon}\eta_k \ . \tag{25}$$

Ψ is then such that

$$\begin{aligned}\frac{\partial\Psi}{\partial\eta_k}+\sum_a \mathcal{D}_a\eta_k&=\frac{\mu_k^A-\mu_k^B-\delta\mu}{2\varepsilon}\ ,\\ \frac{\partial\Psi}{\partial p_k}-\sum_a \mathcal{D}_a p_k&=\frac{\mu_k^A+\mu_k^B-2\mu}{2\varepsilon}\ .\end{aligned} \tag{26}$$

In quasistatic situations, the chemical potential μ and the unbalance $\delta\mu$ between sublattices A and B will be chosen such that

$$\mu=\frac{\mu_k^A+\mu_k^B}{2}\ ,\quad \delta\mu=\frac{\mu_k^A-\mu_k^B}{2}\ . \tag{26a}$$

We shall first show that in one-dimensional profiles, the domains can in principle be obtained using an area-preserving map, as in the case of spinodal decomposition [9]. When we consider a *one-dimensional equilibrium problem along a direction* (with abscissa k), in which the other $(d-1)$ directions are translational invariants (planar antiphase boundaries), the discrete Laplacian functions in (26) reduce to discrete second derivatives in k

$$\begin{aligned}p_{k+1}-2p_k+p_{k-1}&=+\frac{\partial\Psi}{\partial p_k}\ ,\\ \eta_{k+1}-2\eta_k+\eta_{k-1}&=-\frac{\partial\Psi}{\partial\eta_k}\ ,\end{aligned} \tag{27a}$$

with the equilibrium condition

$$\mu_k^A\equiv\mu_k^B\equiv\mu\ ,\quad \delta\mu=0\ . \tag{27b}$$

Equations (27a) present some similarities with an equation of motion in a potential Ψ (fundamental law of the dynamics with on the left-hand side discrete second derivatives with respect to k assimilated to a time); however, the right-hand sides are not the components of a gradient, due to the different signs. Comparison with a motion in the $\{p_k,\eta_k\}$ space can nevertheless help. A surface Ψ is represented in Fig. 5 (for a value of T smaller than T_c). The surface Ψ is invariant by the changes $\eta\to-\eta$, and $\{\mu\to-\mu, p\to 1-p\}$.

As in [9] the ordered domains can be obtained using an area-preserving map

$$\begin{aligned}p_{k+1}&=2p_k+\frac{\partial\Psi}{\partial p_k}-q_k\ ,\\ q_{k+1}&=p_k,\\ \eta_{k+1}&=2\eta_k-\frac{\partial\Psi}{\partial\eta_k}-\chi_k\ ,\\ \chi_{k+1}&=\eta_k\ .\end{aligned} \tag{27c}$$

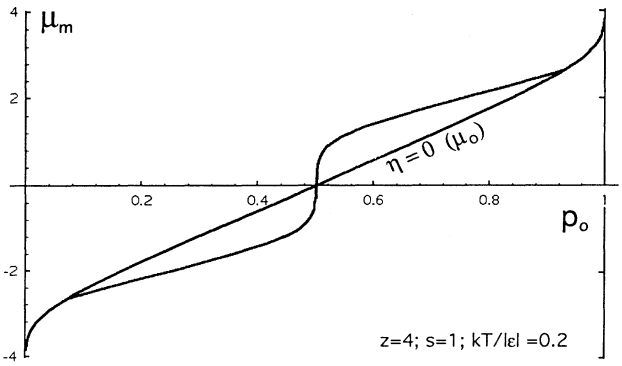

FIG. 4. Variation of the chemical potential μ_m, as a function of p_0. The curve $\eta=0$ corresponds to the chemical potential (μ_0) in the absence of ordering transition (undercooling).

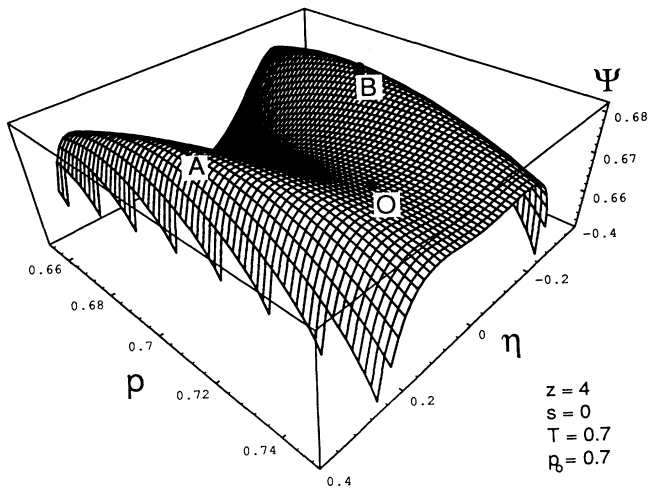

FIG. 5. "Grand potential surface" $\Psi(p,\eta)$ at a temperature smaller than T_c ($\varepsilon=-1$, $z=4$, $s=0$, $p_0=0.7$, $kT=0.7$; here $kT_c=1$). The points A and B are associated with the two equilibrium ordered structures. O corresponds to the unstable (uniform) disordered structure.

A. Small amplitude metastable states

Suppose that we quench a system with concentration p_0, from high temperature to a $T<T_c$: The system reaches an unstable state with uniform chemical potential μ_0 [given by (23)]. Let us first show that, except for very particular cases, it will never encounter small amplitude metastable states around the point $\{p_0,\eta=0\}$. For a given $\mu=\mu_0$ the uniform solutions of (26) correspond to

$$\frac{\partial\Psi}{\partial p_k}=\frac{\partial\Psi}{\partial\eta_k}=0, \tag{28}$$

the solutions of which are

$$\eta_k\equiv 0\ ,\quad p_k\equiv p_0, \tag{28a}$$

corresponding to the thermodynamically unstable point, and

$$\eta_k\equiv\eta_{\rm eq}(\mu_0)\ ,\quad p_k\equiv p_{\rm eq}(\mu_0)\ , \tag{28b}$$

related to Eqs. (17c) and (18) corresponding to the thermodynamically stable points.

Ψ can then be expanded around the "equilibrium" position $\{p_0,\eta=0\}$ of the equivalent dynamical problem (26a) (we set $\varepsilon=-1$ in the following):

$$\Psi(p_0+x,y)=\frac{z+s}{2}(p_0-\tfrac{1}{2})^2-kT\ln(1-p_0)-\left[\frac{z+s}{2}+\frac{kT}{2p_0(1-p_0)}\right]x^2+\left[\frac{z-s}{2}-\frac{kT}{2p_0(1-p_0)}\right]y^2+\dots . \tag{29}$$

For this small amplitude approximation, the right-hand side of Eq. (26a) can be associated with a virtual force derived from the parabolic potential in Eq. (29). In this limit case exact solutions of (26a) can be obtained. They are of the form [19]

$$p_k=\alpha A^k+\beta A^{-k}\ ,\quad \eta_k=\gamma B^k+\delta B^{-k}\ , \tag{30}$$

A and B being solutions of

$$A^2-2(1-a)A+1=0\ , \tag{30a}$$

$$B^2-2(1-b)B+1=0\ , \tag{30b}$$

where

$$a=\left[\frac{z+s}{2}+\frac{kT}{2p_0(1-p_0)}\right]\ ,$$

$$b=\left[\frac{z-s}{2}-\frac{kT}{2p_0(1-p_0)}\right]\ .$$

It is shown in Appendix B that the solutions of (30a) and (30b) do not allow small amplitude equilibrium states, except for very particular systems.

B. Large amplitude metastable states with planar interfaces

We have no general analytic solutions for the concentration profiles. Metastable states (metastable because an infinitesimal density fluctuation could be sufficient to destabilize the system) correspond to given values of the chemical potential μ, and a fixed average concentration p_0.

Let us consider first planar interfaces that are one-dimensional structures varying along the direction k (the $d-1$ other directions being translational invariant). The profiles in $\{p_k,\eta_k\}$ are defined by the discrete Eqs. (27a) or by the map (27c). However, due to the instability of the recursion, it is in practice not possible to simply iterate these equations, starting from given initial conditions $\{p_0,\eta_0\}$ and $\{p_1,\eta_1\}$. One direct way consists in simulating the master Eq. (4), starting for instance from a one-dimensional periodic concentration profile. The local chemical potentials rapidly relax towards a uniform value. The profile of p_k^A of such a metastable state is represented in Fig. 6. It corresponds to a trajectory along AOB on the Ψ surface (Fig. 5). The trajectory of the $\{p_k,\eta_k\}$ follows the curve $\mu=\mu_1=$const derived from Eqs. (14a) and (14b) or Eqs. (26) and (26a),

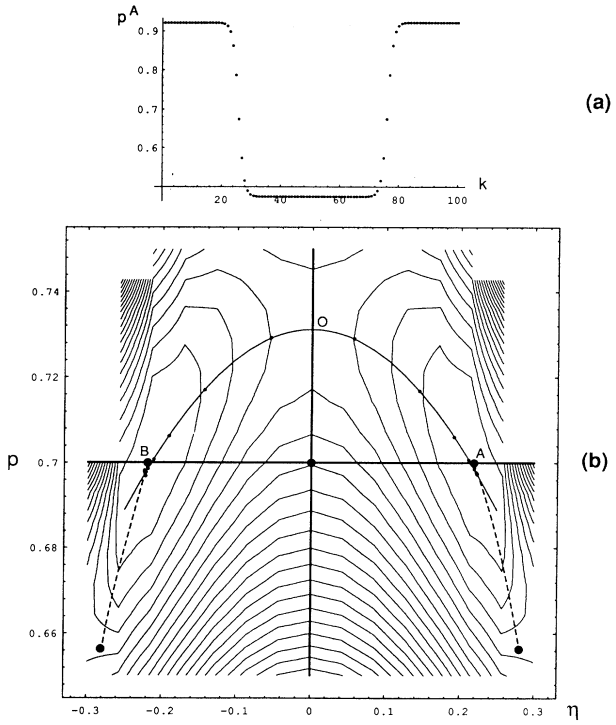

FIG. 6. (a) Equilibrium profile of an A-B strip (the B domain is for $25<k\leq 75$). Periodic boundary conditions are imposed along k. (b) $p(\eta)$ diagram of the above profile ($\varepsilon=-1$; $z=4$; $s=0$; $p_0=0.7$; $kT=0.7$). The Ψ surface, with a chemical potential equal to $\mu_1=1.610\dots$ slightly smaller than μ_m is superimposed (shown by its level lines). The accumulation points are close to A and B, and on the dashed lines representing the homogeneous equilibrium curves $p_{\rm eq}(\eta)$. The middle O of the interfaces corresponds to $\eta=0$ and $p=p_m\cong 0.73$. The line $p=p_0=0.7$, is a center of masses for concentrations of the points on the profile. The solid line corresponds to the curve $\mu(p,\eta)=1.610\dots$ [Eqs. (14), (21), and (23)], and is indistinct from a parabolic fit.

$$\mu=\frac{\mu_k^A+\mu_k^B}{2}=-(z+s)\varepsilon(p_k-\tfrac{1}{2}) -\varepsilon\sum_{a'}\mathcal{D}_{a'}p_k+\frac{kT}{2}\ln\frac{p_k^2-\eta_k^2}{(1-p_k)^2-\eta_k^2} . \tag{31a}$$

The second Equation in (26a) gives the second constraint for the equilibrium profile,

$$\delta\mu=\frac{\mu_k^A-\mu_k^B}{2}=(z-s)\varepsilon n_k+\varepsilon\sum_{a'}\mathcal{D}_{a'}\eta_k +\frac{kT}{2}\ln\frac{(p_k+\eta_k)(1-p_k+\eta_k)}{(p_k-\eta_k)(1-p_k-\eta_k)}\equiv 0 . \tag{31b}$$

In the case of a single kink at equilibrium in an infinite medium, corresponding to $\mu_m=\mu(p_0,\eta)$, A and B are accumulation points and O corresponds to the point $\{p_m,0\}$.

In the vicinity of O, (31b) gives a relation between the discrete Laplacian and the order parameter, and we define the wave vector q by

$$-2q^2=\lim_{\eta_k\to 0}\frac{1}{\eta_k}\sum_{a'}\mathcal{D}_{a'}\eta_k=-(z-s)-\frac{kT}{\varepsilon p_m(1-p_m)} . \tag{32}$$

In the absence of an exact solution for η_k we can consider a hyperbolic tangent form as a good approximation for the single kink profile. η_k can then be written

$$\eta_k\approx\eta_{eq}(p_0)\tanh(qk) , \tag{33}$$

with q given by (32).

The width of the interface varies like q^{-1}, that is, [Eq. (32)] like $[T-T_m(T)]^{-1/2}$, with $T_m(T)=-\varepsilon(z-s)p_m(T)[1-p_m(T)]$ which, when $p_0=p_m=\frac{1}{2}$, is equal to T_c. This is the expected behavior for a nonconserved order parameter [11].

Another convenient approximation concerns the parabolic fit $p(\eta)$ of (31a) shown in Fig. 6. For a single kink profile, the parabola AOB has the expression

$$p=p_m-(p_m-p_0)\left[\frac{\eta}{\eta_{eq}(p_0)}\right]^2 . \tag{34}$$

To determine p_m, related to the amount of defects in the antiphase boundary, we can use Eq. (31a) around O. As the discrete Laplacian of p remains always a small quantity, p_m is given in first approximation by Eq. (22). To improve this result, we calculate $\sum\mathcal{D}_a p_k$ from Eq. (31a) and from Eqs. (34) and (35). This leads to an implicit equation between p_m, p_0, and p_m^0 via Eq. (22). We find

$$p_m=p_m^0+\delta p_m ,$$

with

$$\delta p_m=\frac{(p_m^0-p_0)k(T_m^0-T)}{2[kT-\varepsilon s p_m^0(1-p_m^0)]} , \tag{35}$$

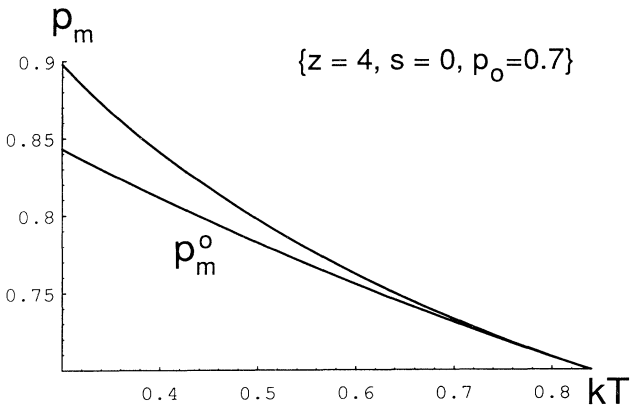

FIG. 7. Graphs of the order parameter η, and of the average concentration p_m as a function of temperature ($\varepsilon=-1$, $z=4$, $s=0$, $p_0=0.7$). (p_m-p_0) gives the excess of defects in the antiphase boundaries, compared to the homogeneous region. The lower curve gives the order zero approximation p_m^0 [Eq. (22)], the upper curve gives a first-order correction [Eq. (35)].

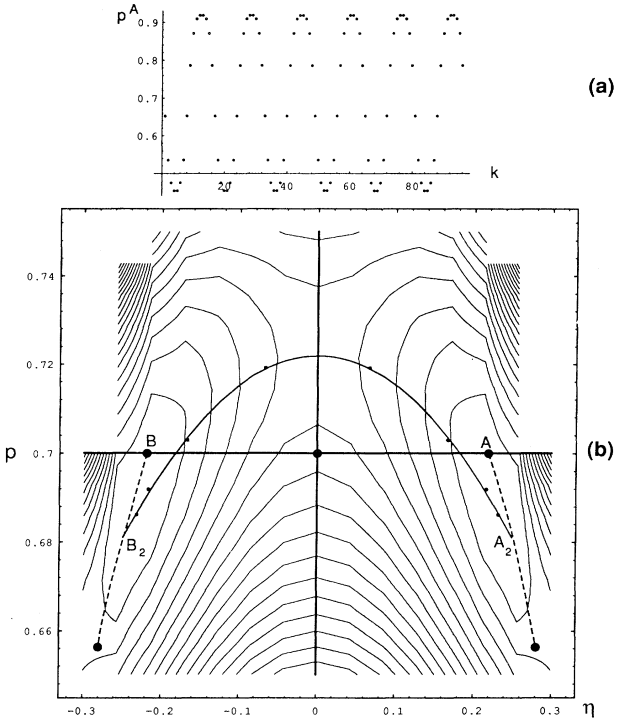

FIG. 8. (a) Equilibrium profile of an A-B periodic strip (each domain has a width of 8 lattice spacings). (b) Same diagram as in Fig. 6. But now there exists no wide enough uniform domains with an equilibrium concentration. As a consequence the parabolas do not go through the equilibrium points A, O, and B associated with the chemical potential μ_m (or μ_1, as in Fig. 6). Here the chemical potential is $\mu_2=1.534\ldots$ corresponding to an ordered homogeneous domain with concentration $p_2\cong 0.676$, and the points A_2 and B_2.

where

$$kT_m^0 = -\varepsilon(z-s)p_m^0(T)[1-p_m^0(T)] .$$

The correction to p_m^0 is of order 0.002, in the example of Fig. 6 ($p_0=0.7$, $p_m^0=0.7293$, $\delta p_m=0.0019$). The general behavior of p_m as a function of T is shown in Fig. 7 in the case $p_0=0.7$. The correction (35) is valid if T is not too small.

In fact, in the case of periodic profiles, as in Fig. 6, where periodic boundary conditions are imposed, $\mu=\mu_1\approx 1.610$ [while $\mu_m(p_0)=1.622$] and the two phases have a concentration slightly smaller than p_0. A metastable state with a shorter wavelength is shown in Fig. 8, for which $\mu=\mu_2\approx 1.535$ is even smaller. But Fig. 9 shows a quasistatic state for which the $\mu_1\approx 1.610$ is imposed by the greater domains, and is then very similar to the case of Fig. 6. However, this state very slowly evolves and the surface of the smaller domain decreases with time (practically linearly). The solid "parabolic" curves in Figs. 6, 8, and 9 are the curves $\mu(p,\eta)=$const.

As we have already noticed, an excess of defects is present in the antiphase boundary (excess of particles: $p_m>p_0$ when $p_0>\frac{1}{2}$, or excess of vacancies: $p_m<p_0$ when $p_0<\frac{1}{2}$). This is a common phenomenon which directly appears in this mean-field approach.

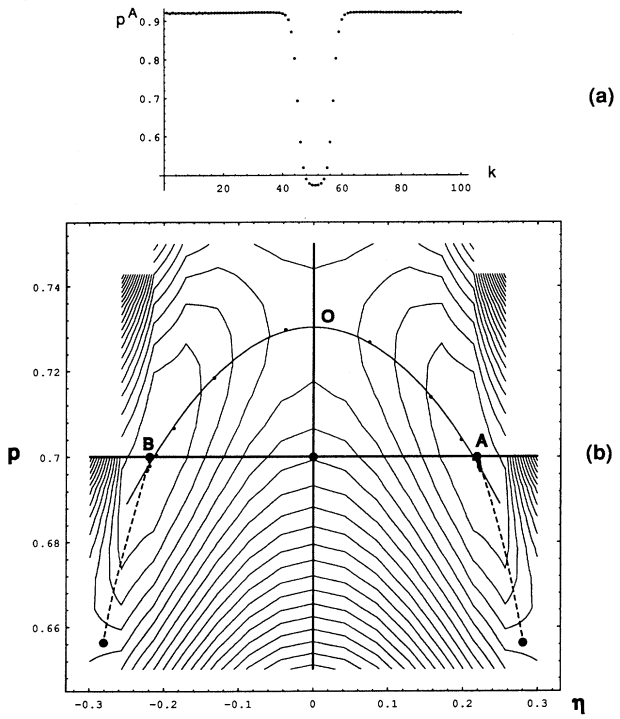

FIG. 9. (a) Equilibrium profile of an A-B asymmetric strip (the B domain is for $45<k<57$). (b) Same diagram as in Figs. 6 and 8. Here the narrow B domain has a width similar to the B domains in Fig. 8, but the A domain is wide enough to be close to the equilibrium homogeneous situation. The diagram is then very similar to Fig. 6(b) (except for the dissymmetry between A and B), and has a chemical potential $\mu_3=1.610\cdots$. The state is in fact quasistatic, and slowly evolves towards a homogeneous A phase.

The excess free energy γ per unit area for a planar interface can also be easily determined. From (19) we obtain

$$\gamma = -\frac{\varepsilon}{a^2}\sum_k\sum_a[(\mathcal{D}_a\eta_k)^2-(\mathcal{D}_a p_k)^2] . \tag{36}$$

In this expression the discrete gradient of p appears to be a negligible quantity, and (36) takes then the usual form of the continuous limit of an integration of the square of the gradient of order parameter normal to the interface.

V. THE ORDER-DISORDER DYNAMICS

We have now all the elements to examine the dynamics of this order-disorder transition after a quench of a high temperature disordered state at a concentration p_0. These dynamics have been simulated using the mean-field equations established above.

The mean concentration $\langle p_k\rangle$ over the whole lattice is a *conserved quantity*. From Eqs. (4) and (11), we see that the equation of evolution of the mean concentration p_k is

$$\frac{\partial p_k}{\partial t} = -\sum_j\{S_{kj}^{AB}(C_j^B-C_k^A)+S_{kj}^{BA}(C_j^A-C_k^B)\} , \tag{37}$$

so that

$$\frac{\partial}{\partial t}\left[\sum_k p_k\right] = -\sum_{k,j}\{S_{kj}^{AB}(C_j^B-C_k^A)+S_{kj}^{BA}(C_j^A-C_k^B)\} \equiv 0 . \tag{38}$$

In the case of a centrosymmetric lattice with nearest neighbor jumps, the evolution equation of p_k can even be written as a discrete divergence of a current

$$\frac{\partial p_k}{\partial t} = -\sum_a \mathcal{D}_a J_{k-a,k}^{AB} . \tag{39}$$

On the contrary, the order parameter η_k is a *nonconserved quantity:*

$$\frac{\partial \eta_k}{\partial t} = -\sum_j\{S_{kj}^{AB}(C_j^B-C_k^A)-S_{kj}^{BA}(C_j^A-C_k^B)\} \tag{40}$$

does not possess any sum rule.

A. Evolution of a circular (or spherical) domain

The surface of a domain is expected in the case of a nonconserved order parameter to evolves at a *velocity proportional to the local curvature* [11],

$$v = -\frac{\alpha^2}{2R} . \tag{41}$$

Starting from Eqs. (38) and (40), it is possible to calculate the evolution of a curved interface. We start from a spherical domain [and a continuous approximation of (38) and (40)] and look at the evolution $\partial p(R,t)/\partial t$ and $\partial\eta(R,t)/\partial t$. The velocity v of the interface is obtained

for profile η in a moving frame ($\eta(R,t) \Longrightarrow \eta(R+vt)$), looking to the points $\{\eta(R,t)=0,\ \eta''(R,t)=0, p'(R)=0\}$ of the interface. A remarkable fact is that the problem is independent on the evolution Eq. (37) of $\partial p(R,t)/\partial t$, hence of the explicit values of p.

We have made the calculation in two cases, the square ($z=4$) and the simple cubic lattice ($z=6$). We obtain expressions of the form (41), that is,

$$v = 4w_0 e^{-(4-s)(\varepsilon/kT)p_0}\left[1+(12-s)\frac{\varepsilon}{kT}p_0(1-p_0)\right]\frac{1}{R} \quad \text{when } z=4\ , \tag{42a}$$

and

$$v = 8w_0 e^{-(6-s)(\varepsilon/kT)p_0}\left[1+(18-s)\frac{\varepsilon}{kT}p_0(1-p_0)\right]\frac{1}{R} \quad \text{when } z=6\ . \tag{42b}$$

The above velocities are always negative as long as the set $\{p_0, kT\}$ is inside the ordered region: The radius of circular or spherical domains then *decreases* like the square root of time [11]

$$R(t) = \alpha\sqrt{t_0 - t}\ . \tag{43}$$

This behavior is also well verified numerically: the evolution of R is shown in Fig. 10. A discrepancy only appears when the radius becomes of order of the width of the interface. It can be also noticed that the prefactors of $1/R$ in (42a) and (42b) contain two terms: only the second, with the general form, $(a/kT)p_0(1-p_0)\exp\{-p_0(z-s)\varepsilon/kT\}$ is proportional to the mobility {see Eq. (19) in [11]}, as is expected in a phenomenological approach (the mobility is easily obtained *in first approximation* using Eq. (11″) together with (12a) and (12b) and the constraint $p_i^A \equiv p_i^B \equiv p_0$). When the two terms are taken into account, it can be observed that the velocity reaches the value zero inside the disordered region (where v has no meaning) and remains negative on the phase transition curve [defined by $kT = -(z-s)\varepsilon p_0(1-p_0)$].

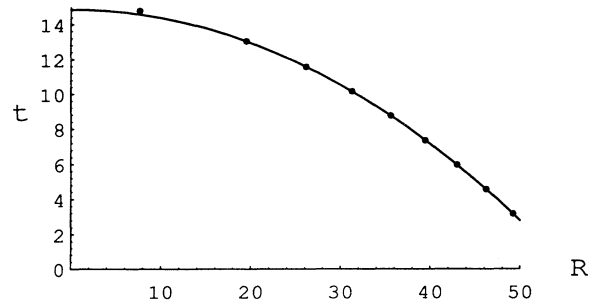

FIG. 10. Time evolution of the radius of a spherical droplet. We find numerically $t = 14.86 - 0.004\,82R^2$. The usual law of evolution in $\sqrt{t}$ of droplets in the case of a nonconserved order parameter is obtained. The analytical approximation (42a) would give a coefficient of R^2 equal to -0.0035.

B. Global evolution of a quenched sample

As an example we have followed the evolution with time of a (relatively small) sample of size 100×100, starting at $t=0$ from a homogeneous high temperature disordered distribution with a concentration p_0. At $t=0$, a small noise ($-10^{-5} < \delta\eta < 10^{-5}$) is added, via the order parameter, to this uniform concentration. At $t>0$, most of the sample goes far from the unstable point so that the effect of a noise can be neglected.

The sequence in Fig. 11 shows the evolution of the system in the representation space $\{p_k, \eta_k\}$. At time $t=0$, the various sites of the sample are all located in the close vicinity of the point $\{p_0, 0\}$, and their chemical potential is μ_0 [Eq. (23)]. After the quench the system evolves at the beginning exponentially. At $t=1$ (arbitrary units of time), parabolic structures indicate that local chemical potential equilibrium has been attained, with incipient phase and boundaries. At $t=2$, large regions of the sample have reached their equilibrium, corresponding to sites on the equilibrium curve $p_{eq}(\eta, T)$ [Eq. (18)]. They are separated by antiphase domains, but the width of the parabolic distribution shows that the chemical potential is not homogeneous or equivalently that, on a mesoscopic scale, the concentration is not homogeneous. The values of the chemical potential can be obtained from Eq. (22), where the distribution of p_m corresponds to $\eta=0$. At $t=7$, the amount of sites in an equilibrium situation has increased [Fig. 12 shows the general distribution of $\eta(x,y)$ and $p(x,y)$]. The points above the main parabola which are located in the $\eta<0$ region correspond to the disappearance of A domains (they form incomplete parabolas). Then the sample becomes more and more homogeneous ($t=25$). At $t=50$, the distribution presents an asymmetric structure: most of the particles are now on B domains and the asymmetry of the parabola with respect to η can be associated with linear gradients of chemical potential in the η space. This behavior is clearly visible in Fig. 13. At $t=64$, only one ordered phase (B) remains in the 100×100 sample, but if η has reached its equilibrium everywhere the concentration is still not at its equilibrium value p_0, and p varies in the range $0.698 \le p \le 0.706$. Long distance diffusion of matter is now necessary to reach the final equilibrium.

C. Conductivity in the ordered regions and in the antiphase boundaries

The conductivity σ can be easily determined from the linear response to an electric field δE. We find from

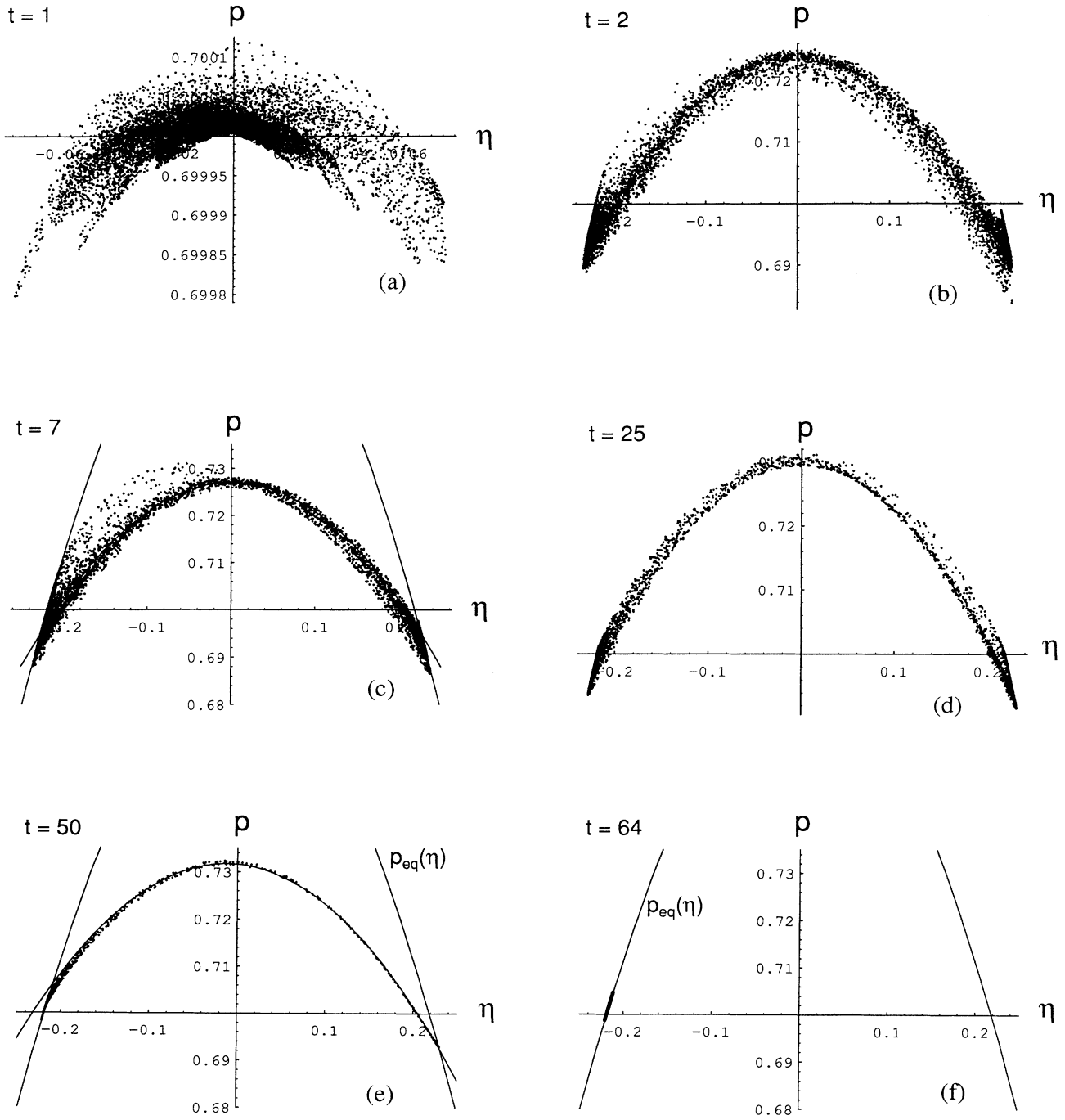

FIG. 11. These figures show the evolution of the distribution of values $\{\eta,p\}$ in a sample of size 100×100. At $t=0$, the system is quenched from a uniform disordered configuration at large temperature to a $T<T_c$. The time unit is arbitrary. The system starts from the configuration $\{p=p_0,\eta=0\}$, to which a small noise has been added ($|\delta\eta|<10^{-5}$). (a) At $t=1$, some parabolic structures are already visible (existence of small regions of homogeneous chemical potential). During this initial period the evolution is exponential. (b) At $t=2$, the points are distributed on various parabolas, and regions of equilibrium $\{\eta_{eq},p_{eq}\}$ have been reached (the chemical potential $\mu=$const, depending only on the mesoscopic average concentrations). (c), (d), and (e) The domain boundaries become better and better defined. The width of the parabola distribution becomes narrower. In (c), we see a set of points with a larger concentration, located only in the upper-left quadrant. They correspond to a disappearing A domain (centered around $x=100$, $y=80$ in Fig. 12). The main distribution follows roughly a parabola (solid line). The curve $p_{eq}(\eta)$ is a place of accumulation of ordered regions with a $0.685<p<0.71$. In (e), we see that most of the points are on B domains; in addition the parabola is asymmetric, indicating the existence of a small gradient of chemical potential between A domains and B domains. (f) The interfaces have all disappeared, and only phase B remains. All the points are now on the curve $p_{eq}(\eta)$. However, the concentration is not yet homogeneous. Gradients of defects are present in the system. Their evolution is now only driven by diffusion.

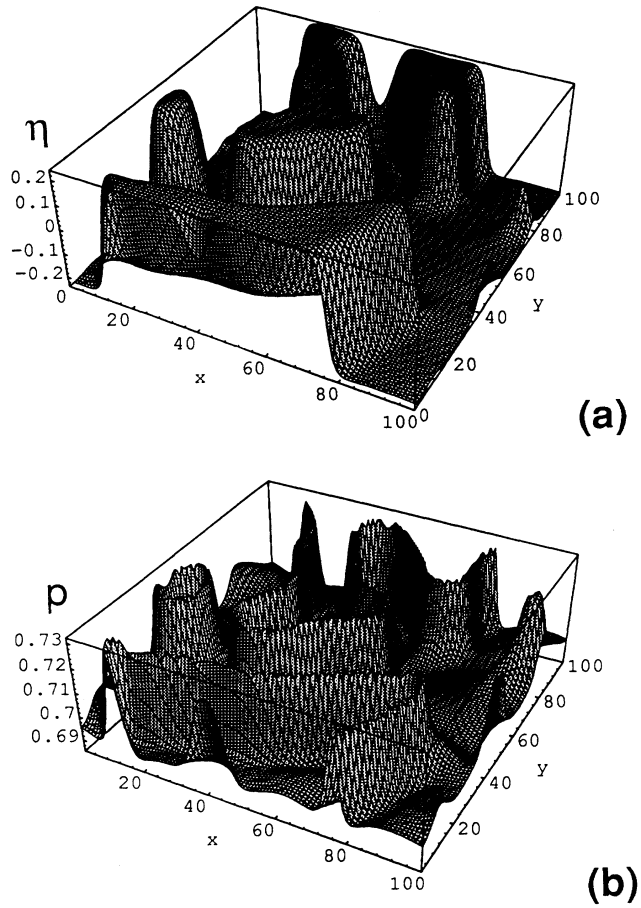

FIG. 12. (a) Surface $\eta(x,y,t)$ at time $t=7$ [Fig. 11(c)]. (b) Surface $p(x,y,t)$ for the same configuration, showing the enhancement of defects in the interfaces.

$$\sigma=\delta J/\delta E$$

$$\sigma_{ij}^{AB}=\frac{1}{kT}S_{ij}^{AB}(C_i^A+C_j^B)\ . \tag{44}$$

In Fig. 14, we see that the presence of defects (particles or vacancies) in the antiphase boundaries raises the conductivity: The numerical simulation has been performed in a layer of domains A and B as in Fig. 6. Its conductivity $\sigma^{AB}=\sigma^{BA}$ shows an increase from 0.021 to 0.035 in the direction parallel to the interfaces, and in the direction perpendicular to the interfaces, σ^{AB} shows an increase from 0.021 to 0.023 if $\text{grad}p^A<0$ and from 0.021 to 0.053 $\text{grad}p^A>0$ (and the reverse for σ^{BA}). In the direction normal to the interface a contribution of the gradient of concentrations (p^A or p^B) must be added to σ^{AB} (or σ^{BA}). The average conductivity is indeed given by $\sigma=(\sigma^{AB}+\sigma^{BA})/2$.

In addition we can see that the conductivity has

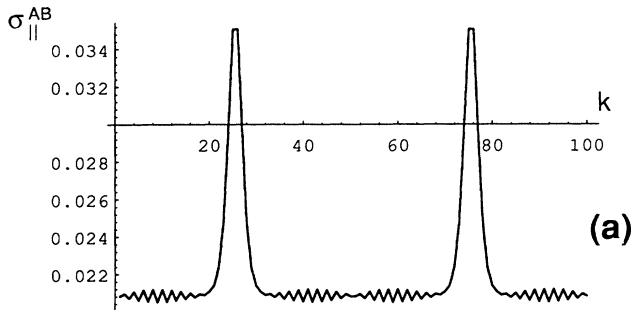

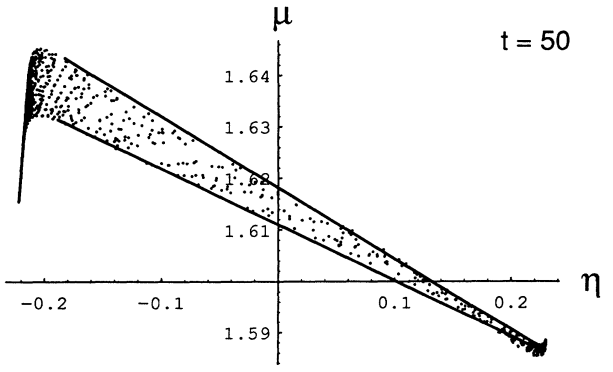

FIG. 13. Distribution of chemical potential μ as a function of η, at time $t=50$, when the relation $p(\eta)$ follows an asymmetric parabola [Fig. 11(e)]. It shows clearly linear dependencies of $\mu(\eta)$ through the antiphase boundary. The "parabola" $p(\eta)$ given by Eq. (31a) now contains a linear term in η explaining the asymmetry of the parabola.

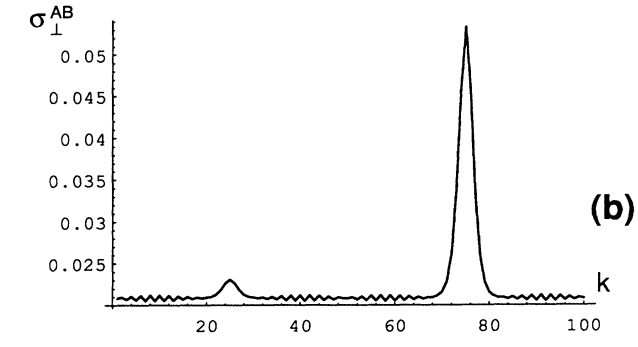

FIG. 14. (a) Conductivity $\sigma=\sigma_{\parallel}^{AB}=\sigma_{\parallel}^{BA}$ in the direction parallel to the interface, determined in the case of the A-B strip of Fig. 6. (b) Conductivity σ^{AB} in the direction normal to the interface; the conductivity from sublattice A to sublattice B contains an odd contribution in $\text{grad}p^A$ but $\sigma=(\sigma^{AB_\perp}+\sigma^{BA_\perp})/2$.

(within 1% in the numerical example) in the direction parallel to the interface, the general form

$$\sigma^{AB}_{\mathbf{k},\mathbf{k}+\mathbf{a}}=\sigma_0-\sigma_1 p_{\mathbf{k}}(1-p_{\mathbf{k}}) \tag{45a}$$

which leads in the presence of a variation δp of the defects in the interfaces, to an enhancement of the conductivity,

$$\delta\sigma\approx\sigma_1(2p_{\mathbf{k}}-1)\delta p \ . \tag{45b}$$

This effect of negative resistance at interfaces has been also recently noticed by Maugis and Martin [20]. The mean conductivity can be estimated, at least in first approximation: If we consider the conductivity in the interface ($\eta=0$) for a system with a homogeneous concentration p_0, then (44) is two times the average mobility calculated from (11''): $\sigma^{AB}\approx 2w_0\exp[-p_0(z-s)\varepsilon/kT]p_0(1-p_0)$.

VI. CONCLUSION

To summarize, we have shown that starting from the master equation describing the evolution of a repulsive particle (here nearest neighbor interaction and nearest neighbor jumps), the most natural mean-field approximation leads to Allen-Cahns type equations. These Allen-Cahn equations are generalized equations in the sense that, far from equilibrium, they are as valid as the mean-field approximation is. In the present case (square and simple cubic lattices) we have found a set of two coupled equations linking the order parameter and the mean local concentration. It is remarkable that in these equations it is possible to identify chemical potentials which could be deduced from the natural inhomogeneous free energy function. The calculations have been greatly simplified by the use of the simultaneous evolution of the two possible sublattice histories, allowing one to define local parameters on the same site. We have used these equations to study some interesting physical features: the evolution of a curved antiphase boundary, the concentration of defects in the boundaries, and the variation of the conductivity inside and outside a boundary, showing an enlargement of the conductivity in the interfaces, a result which has recently been observed [20]. We have examined the global evolution of a 100×100 sample, showing the various time scales of the evolution, appearance of domains, evolution of these domains, presence of quasiconstant gradients of chemical potentials through the interfaces, and final evolution by diffusion of the inhomogeneities of concentration. As in the case of attractive interaction, the method allows us to calculate explicit expressions for the mobility, the interface velocity, the conductivity (in the limit of validity of mean field). The interest of the approach is its wide generality of application: it is clear for instance that it also applies to master equations with longer ranges of interactions and to more complicated lattice structures.

Note added. While this paper was in revision, Professor Georges Martin transmitted to me two manuscripts [21,22] which deal with the same subject, using a slightly different approach but leading to similar results.

ACKNOWLEDGMENTS

The preliminary work of this paper has been done by Jean-Pierre Pujol, in the course of a short stay in our group. Here, his collaboration is acknowledged. I also thank Max Kolb, Wolfgang Dieterich, Georges Martin, and Bernard Legrand for many fruitful discussions. Laboratoire de Physique de la Matière Condensée is Unité de Recherche D-1254 Associée au Centre National de la Recherche Scientifique.

APPENDIX A

To avoid complicated expressions involving sublattices A and B, for which the concentration is not taken on the same site, it appears very useful to have quantities belonging to different colors but taken on the same sites. To understand why this is possible, it is necessary to examine in more detail the evolutions of the concentrations.

Let us consider two independent (one-dimensional to simplify) systems with initial conditions defined following Fig. 15(a). At time $t=0$, the black dot configuration is a quasihomogeneous configuration with

$$p_1^A=p_0+\delta\eta_1 \ , \quad p_2^B=p_0-\delta\eta_2 \ , \ldots \ ,$$

where $\delta\eta_i$ are very small fluctuations (this is for instance a high temperature disordered configuration, quenched below T_c at $t=0$). This configuration is a realistic state which will evolve with time with the creation of ordered regions of colors A and B. Now together with this configuration we consider the white dot configuration with

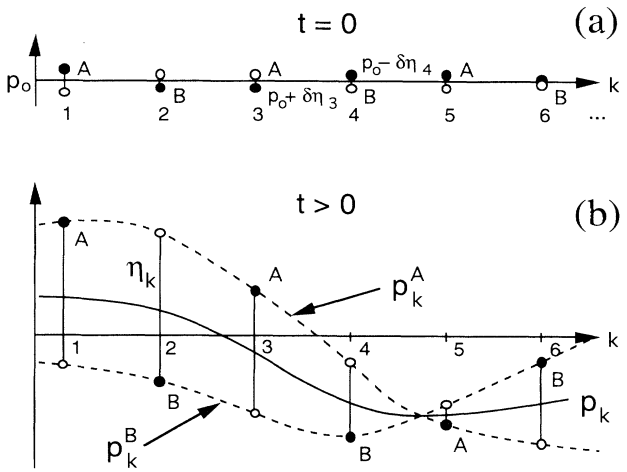

FIG. 15. Definition of sublattice variables on each lattice site $\mathbf{k}$. (a) Initial conditions: At time $t=0$, the system consists in a high temperature disordered state, with an average concentration p_0 to which very small fluctuations $\{\delta\eta_{\mathbf{k}}\}$ are superimposed on each site. Two realizations are shown, the first with concentrations $\{p^A,p^B\}$ indicated by black dots, the second with concentrations $\{p'^A,p'^B\}$ indicated by white dots and symmetrical (at $t=0$) of the first with respect to p_0. (b) After a quench ($T<T_c$) at $t=0$, the two realizations evolve with time and are such that the sets $\{p_1^A,p_2'^B,p_3^A,\cdots\}$ and $\{p_1^B,p_2'^A,p_3^B,\cdots\}$ remain smooth functions of the position $\mathbf{k}$.

$$p_1'^A = p_0 - \delta\eta_1 \ , \quad p_2'^B = p_0 + \delta\eta_2 \ , \quad \ldots \ ,$$

which is obtained from the black configuration, by changing $\delta\eta_i$ into $-\delta\eta_i$; and in addition we identify the p'^A with a p^B and p'^B with a p^A:

$$p_1^B = p_0 - \delta\eta_1 \ , \quad p_2^A = p_0 + \delta\eta_2 \ , \quad \ldots \ .$$

We now claim that when the time increases, while the two configurations evolve completely independently, the sequences

$$p_1^A \ , \ p_2^A \ , \ p_3^A \ , \ldots \text{ and } p_1^B, \ p_2^B, \ p_3^B \ , \ldots$$

are smooth functions of the position k as shown in Fig. 15(b). In the example of the figure, the black configuration is of "color" A for $k \leq 4$ ($p^A \leq p^B$) and of color B for $k \geq 5$.

The reason for this claim comes from the evolution of Eqs. (37) and (40). One can verify that their right-hand side is even in the order parameter η, so that the solutions for the black and white configurations are of the form

$$p_k^A = p_k + \eta_k + \delta\eta_k' \ , \quad p_k^B = p_k - \eta_k - \delta\eta_k'' \ .$$

Both solutions p_k and η_k of Eqs. (37) and (40) being smooth in the coordinate k (the noise $\delta\eta_k'$ and $\delta\eta_k''$ being negligible), this is also true for p^A and p^B. This is not a rigorous mathematical proof of the assertion of this appendix, of course. Nevertheless each step of our arguments is reasonable, and the conclusions are confirmed by numerical results.

APPENDIX B

Existence of ordered regions imposes $b \geq 0$, or

$$kT \leq (z-s)p_0(1-p_0) \leq kT_c = (z-s)/4 \ . \tag{B1}$$

1. Solutions for p_k

(i) If $0 \leq a \leq 2$, we can set $(1-a) = \cos\phi$, in (30a); this leads to oscillatory solutions for p_k:

$$p_k = p_0 + 2\alpha \cos k\phi \ , \tag{B1a}$$

which is possible if

$$kT \leq (4-z-s)p_0(1-p_0) \leq kT_p = (4-z-s)/4 \ .$$

(ii) If $2 \leq a$, we can set $(1-a) = \cosh u$, in (30a); this leads to exponential solutions for p_k:

$$p_k = p_0 + \alpha \exp ku + \beta \exp(-ku) \ , \tag{B1b}$$

which is possible if

$$(4-z-s)p_0(1-p_0) \leq kT \leq (z-s)p_0(1-p_0) \ .$$

This is the case for the square or simple cubic lattices (for which $T_p < T_c$ or $z > 2$). When the lattice is infinite, k takes all values between $-\infty$ and $+\infty$, no small amplitude solutions exist except when $\alpha = \beta = 0$, and then,

$$p_k \equiv p_0 \ .$$

Small amplitude variations of p_k and η_k are possible on chains ($z = 2$) or in square lattices when $s = 1$, and also for finite size systems where k and then (26a) remain bounded.

2. Solutions for η_k

Notice first that b is always positive (ordered region).

(i) If $b \leq 2$, we can set $(1-b) = \cos\theta$, in (30b); this leads to oscillatory solutions for η_k:

$$\eta_k = 2\gamma \cos k\theta \ , \tag{B2a}$$

which is possible if

$$(z-s-4)p_0(1-p_0) \leq kT \leq (z-s)p_0(1-p_0) \ .$$

(ii) If $2 \leq b$, we can set $(1-b) = \cosh v$, in (30b); this leads to exponential solutions for η_k:

$$\eta_k = \gamma \exp kv + \delta \exp -kv \ , \tag{B2b}$$

which is possible if

$$kT \leq (z-s-4)p_0(1-p_0) \ .$$

Again in this case (low temperature region only present in $z > 4$ lattices) no small amplitude solutions exists (existence of abrupt interfaces).

[1] D. de Fontaine, in *Solid State Physics,* edited by H. Ehrenreich, F. Seitz, and D. Turnbull (Academic, New York, 1979), Vol. 34, p. 73.

[2] W. Dieterich, J. Stat. Phys. **39**, 583 (1985), and references therein; Proceedings of the Sixth International Conference on Solid State Ionics, Garmisch, 1987 [Solid State Ionics **28–30** (1988)]; Proceedings of the Eleventh International Symposium on the Reactivity of Solids, Princeton, 1988 [Solid State Ionics **32 and 33** (1989)].

[3] A. J. Berlinsky, W. G. Unruh, W. R. McKinnon, and R. R. Haering, Solid State Commun. **31**, 135 (1979); Y. Chabre and P. Deniard, in *Chemical Physics of Intercalation,* Vol. 172 of *NATO Advanced Study Institute, Series B: Physics,* edited by A. P. Legrand and S. Flandrais (Plenum, New York, 1987), p. 395.

[4] A. G. Naumovets (unpublished); A. A. Tarasenko and A. A. Chumak, Sov. Phys. Solid State **22**, 1716 (1980); **24**, 1683 (1982); A. Sadik and K. Binder, Surf. Sci. **128**, 350 (1983); A. Natori and H. Ohtsubo, Surf. Sci. **171**, 13 (1986); **184**, 289 (1987).

[5] M. Kolb, T. Gobron, J.-F. Gouyet, and B. Sapoval, Europhys. Lett. **11**, 601 (1990).

[6] A. Hekkouri, M. Kolb, and J.-F. Gouyet (unpublished).

[7] J. W. Cahn and J. E. Hilliard, J. Chem. Phys. **28**, 258

(1985); J. W. Cahn, *ibid.* **42**, 93 (1965).
[8] J. D. Gunton, M. San Miguel, and P. S. Sahni, in *Phase Transitions and Critical Phenomena,* edited by C. Domb and J. L. Lebowitz (Academic, London, 1983), Vol. 8.
[9] R. Pandit and M. Wortis, Phys. Rev. B **25**, 3226 (1982).
[10] J. F. Gouyet, Europhys. Lett. **21**, 335 (1993). Note the following misprints in this paper: p. 339, $\mu_1=\partial\langle F\rangle/\partial p_{\mathbf{k}}$; $\mu_{\mathbf{k}}=\mu_0+\mu_1+[(z+s)/2]\varepsilon$, and in Eq. (16)

$$\langle F\rangle=\sum_{\mathbf{k}}\left[\phi_{\mathbf{k}}+\frac{\varepsilon}{2}\sum_{\mathbf{a}}(\mathcal{D}_{\mathbf{a}}p_{\mathbf{k}})^2\right].$$

[The introduction of a relation between the master equation and the Cahn-Hilliard equation was made by G. Martin, Phys. Rev. B **41**, 2279 (1990), treating a one-dimensional case.]
[11] S. M. Allen and J. W. Cahn, Acta Metall. **27**, 1085 (1979).
[12] A. Hekkouri, R. Nassif, M. Kolb, and J.-F. Gouyet (unpublished).
[13] At the interfaces between different ordered regions, the variations will be indeed more important, but we always suppose that the gradients remain much smaller than the inverse lattice spacing.
[14] More exactly it becomes proportional to a Laplacian in the continuous limit, with a coefficient of proportionality which depends on the lattice structure.
[15] M. Nieswand, A. Majhofer, and W. Dieterich, Phys. Rev. E **47**, 718 (1993); **48**, 2521 (1993); D. Reinel, W. Dieterich, and M. Nieswand (unpublished).
[16] R. Fowler and E. A. Guggenheim, *Statistical Thermodynamics* (Cambridge University Press, London, 1960).
[17] H. Sato and R. Kikuchi, J. Chem. Phys. **55**, 677 (1971).
[18] K. R. Subbaswamy and G. D. Mahan, Phys. Rev. Lett. **37**, 642 (1976).
[19] A. O. Gel'fond, *Calculus of Finite Differences* (Hindustan, Delhi, 1971).
[20] P. Maugis and G. Martin, Phys. Rev. B **49**, 11 580 (1994).
[21] G. Martin, Phys. Rev. B **50**, 12 362 (1994).
[22] V. G. Vaks, S. V. Beiden, and V. Yu. Dobretsov (unpublished).